INL/JOU-18-45672-Revision-0

Fuel-Clad Chemical Interaction Evaluation of the TREAT Reactor Conceptual Low-Enriched-Uranium Fuel Element

Clemente J. Parga, Isabella J. van Rooyen, Eric P. Luther

December 2018

The INL is a U.S. Department of Energy National Laboratory
operated by Battelle Energy Alliance

INL/JOU-18-45672-Revision-0

Fuel-Clad Chemical Interaction Evaluation of the TREAT Reactor Conceptual Low-Enriched-Uranium Fuel Element

Clemente J. Parga, Isabella J. van Rooyen, Eric P. Luther

December 2018

Idaho National Laboratory
Idaho Falls, Idaho 83415

http://www.inl.gov

Prepared for the
U.S. Department of Energy

Under DOE Idaho Operations Office
Contract DE-AC07-05ID14517

Fuel – Clad Chemical Interaction Evaluation of the TREAT Reactor Conceptual Low-Enriched-Uranium Fuel Element

C. J. Parga,[1] I. J. van Rooyen,[1*] and E. P. Luther[2]

[1]*Fuel Design and Development, Idaho National Laboratory, Idaho Falls, ID 83415, USA*
[2]*Materials Science and Technology, Los Alamos National Laboratory, Los Alamos, NM 87545, USA*
**Corresponding Author. Distinguished Staff Scientist, Fuel Design and Development, Idaho National Laboratory, Idaho Falls, ID 83415, USA. Email: Isabella.vanrooyen@inl.gov*

Abstract

The Transient Reactor Test (TREAT) facility resides at the Materials and Fuels Complex (MFC) at Idaho National Laboratory (INL). The TREAT reactor is currently undergoing design and engineering studies for its conversion from a high enriched uranium (HEU) to a low-enriched uranium (LEU) core. The conceptual design of the LEU fuel element identified two main design differences compared with the HEU fuel element; namely, it will contain four times more fissionable material in its graphite matrix and distinct nuclear-grade Zirconium alloy, as Zircaloy-3 was used in the HEU fuel assembly and is not commercially available currently. These design changes may impact the magnitude of chemical interaction between fuel and cladding materials during physical contact under expected TREAT operation conditions and, therefore, was evaluated through a combination of experimental testing and thermodynamic modeling in order to determine implications for the fuel assembly. In this study, two potential cladding material types, Zircaloy-4 or Zr-1Nb alloys, were evaluated, and it was found for both material types that the extent of interaction and specific chemical reactions are minimal and no detrimental effect on the overall cladding properties is observed. The resulting interaction layer of 3-6 μm was measured after a 2-week exposure at 820°C. The thermodynamic analysis was extended to temperatures beyond the TREAT reactor operation and accident conditions in order to give some insight that may be of interest for other reactor systems as the High Temperature Gas Reactors (operation above 1,000°C) and for Nuclear Reactor Severe Accident phenomenology study where the UO_2 fuel could reach temperatures over 2,800°C and melt.

Keywords: TREAT Reactor; LEU Fuel; fuel-clad interaction; Experimental; Thermodynamic Modeling

1. Introduction

Testing capacity of advanced fuel and reactor materials under transient conditions became more crucial after events at the Fukushima Daiichi Nuclear Power Plant in March 2011; international focus was directed toward development of accident-tolerant fuels for light-water reactors [1]. The U.S. Department of Energy (DOE) had previously authorized the resumption of operations of the TREAT facility at INL in 2010 [2]. TREAT had successfully operated during a 35-year period until it was put into cold shutdown in 1994, attaining approximately 0.7% burnup. On November 14th, 2017 the TREAT resumption operations were completed and the reactor went through various low-power tests and transient operations up to 12 GWth (gigawatts thermal) utilizing the original HEU fuel.

In harmony with the conversion of many experimental reactors in the U.S.A. and worldwide, the National Nuclear Security Administration (NNSA), through the Office of Material Management and Minimization, the TREAT LEU Conversion Program was initiated. The objective of this project is the designing, qualifying, and fabrication of a new LEU core to substitute the original 60-year old HEU fuel core [3]. The new core will incorporate modern fabrication capabilities, fit the original fuel assembly dimensions, and has been designed to maintain experimental performance capabilities and satisfy operational safety

requirements. The new TREAT LEU core is being engineered to be a lifetime core that will maintain functionality, structural soundness, and safe operation during its projected 40-year service life. The TREAT reactor is a graphite-moderated, air-cooled reactor that was based on HEU (U-235 > 90 wt.% U) U_3O_8 oxide dispersed in a graphite matrix [4].

The LEU (U-235 < 20 wt.% U) conceptual design requires approximately four times more uranium in the fuel than the current HEU design to achieve an equivalent total energy deposition in the test vehicle. The conceptual LEU fuel assembly will consist of stacked ~4-inch square cross section graphite blocks with finely dispersed uranium oxide particles and graphite reflector blocks placed on top and bottom of a columnar assembly. The fuel and graphite reflector blocks are encased in a hermetic metallic cladding that protects them from the exterior atmosphere, contains the fission products, and aids in conduction of heat produced by fission. The conceptual design of the LEU fuel assembly cladding is approximately 2.5-m long with a wall thickness of 0.66 mm (±0.0508 mm); clearance between fuel block and cladding is less than 0.38 mm. Information on the original HEU fuel assembly and finite element analysis of the conceptual LEU fuel assembly design has shown that the cladding sheet bows inward, and 57% of the sheet material is in physical contact with the fuel [5]. Neutronics considerations limit the fuel assembly's cladding material choice to essentially neutron transparent material such as Zr-based alloys (low macroscopic thermal neutron cross-section). The assembly must possess good air oxidation resistance and adequate mechanical strength during steady-state operation (P = 120 kW; T_{fuel} = 278°C), energetic test transients (P = 21 GW/ms; T_{fuel} = 600°C), and design basis reactivity insertion accident (RIA) resulting in a 4.7 GJ total energy release from fission and a respective increase in the fuel temperature up to 820°C [6].

Historic reports on the original TREAT HEU fuel cladding material, Zircaloy-3, indicated no embrittlement or deleterious effect due to interaction with graphite, beside slight discoloration [7,8]. No specific fuel particle-graphite and cladding material in-depth analysis or results were found in the archives. As the LEU fuel cladding will consists of another Zr-based alloy instead of Zircaloy 3, and the source of the fuel may contain impurities due to current fuel supply chain availability, it is necessary to determine if the LEU fuel assembly is compromised due to interaction between the fuel block (graphite and fuel particles) and the cladding down-selected alloy materials (Zircaloy-4 and Zr-1Nb alloy) during reactor operation. Therefore, the fuel-clad chemical interaction (FCCI) study undertaken entails the understanding of the potential interaction between the Zr-based metallic cladding in physical contact with the graphite/urania composite fuel at 820°C temperature and vacuum pressure (0.6 mPa). Multiple interaction scenarios such as diffusion, carburization or carbiding, red-ox reactions, alloying or compound formation and microstructural effects need to be considered and analyzed along with their potential repercussion on the mechanical properties, thermal conductivity, and hermeticity of the conceptual TREAT LEU fuel assembly. Even though the TREAT reactor transients are limited to produce a maximum fuel peak temperature of 600°C, the RIA design basis accident scenario considers a maximum peak temperature of 820°C under this type of nuclear excursion. Hence, the FCCI test was intended to provide an upper boundary on fuel and cladding interaction at 820ºC during a 336-hour period.

This article presents the TREAT LEU fuel element-clad materials' interaction results. The evaluation combines an experimental and computer modeling approach for the understanding of the FCCI complex phenomena. The retrofit of the experimental testing and thermodynamic modeling serve to predict empirical results and validate thermodynamic databases. The characterization of the specimens consisted of scanning electron microscopy (SEM) in backscatter electron and secondary electron imaging (BSE/SE), X-ray diffraction (XRD), nano-hardness testing, computer reconstructed X-ray tomography, image processing and analysis, and materials thermodynamic modeling.

2. Experimental

2.1 Materials and Fabrication Details

The LEU UO_2 fuel powder (19.75 wt.% enrichment; particle size of <44 µm) was purchased from the Y-12 National Security Complex, a DOE NNSA facility in Oak Ridge, Tennessee. The total impurity concentration in the LEU UO_2 amounted to 1450 ppm, being slightly higher than the 1200 ppm specification of the original HEU fuel. Abnormally higher concentrations of Al and Mg were detected in a few large UO_2 agglomerates which lead to the formation of a lamellar interaction zone between the UO_2-Graphite. The contamination was traced back to degradation of the crucible material during UO_2 production, which has been acknowledged and corrected for future batches. The previous publication gives more details on the impurity content in the UO_2. [9]. The fuel pellet was fabricated at Los Alamos National Lab using a mixture of 64 wt.% natural graphite (Asbury Carbons 3482), 16 wt.% synthetic graphite (SGL KRB2000), 19 wt.% novolac phenolic resin (Hexion Durite), and 1 wt.% hexamethylenetetramine (Fisher Scientific). The graphite matrix constituents were jet milled to blend and reduce the average particle size to approximately 10 µm. Subsequently, the LEU UO_2 was added and the mixture was blended in a high shear mixer (CMC DP-1.5 Liter Laboratory Double Planetary Mixer). Isopropyl alcohol was slowly added until the powder began to granulate. The granulated powder was placed under vacuum overnight to remove the alcohol. Afterwards, the granulated powder was placed inside a cylindrical die (25.5-mm diameter) and pre-heated in an oven to 160°C. The powder and die were heated for 5 minutes and then uniaxially pressed to 80 MPa, after which the green compacts were baked in a tube furnace at 950°C (ramp rate of 10˚C/hr) and held for 1 hour under a flowing, gettered argon atmosphere (200 sccm). The sintered samples had a graphite-to-total-carbon ratio of 0.9 and a 1170 carbon-to-uranium ratio.

The fuel sample preparation is displayed on Figure 1. The pellet (Figure 1a) was sectioned (Figure 1b) into eight equally sized “cake slice” pieces (Figure 1c) (height: 9 mm, radius: 11 mm, mass: ~ 1.3 g). The top and bottom of each sample has a 150- and 320-grit sanding paper finish, respectively (more details in [9]). Two cladding alloys were compared in this study namely (1) Zircaloy-4 (Zry-4) sheet (1.6-mm-thick) and (2) nuclear-grade Zr-1Nb alloy sheet (0.66-mm-thick). Table 1 displays the composition of the Zr-alloys studied.

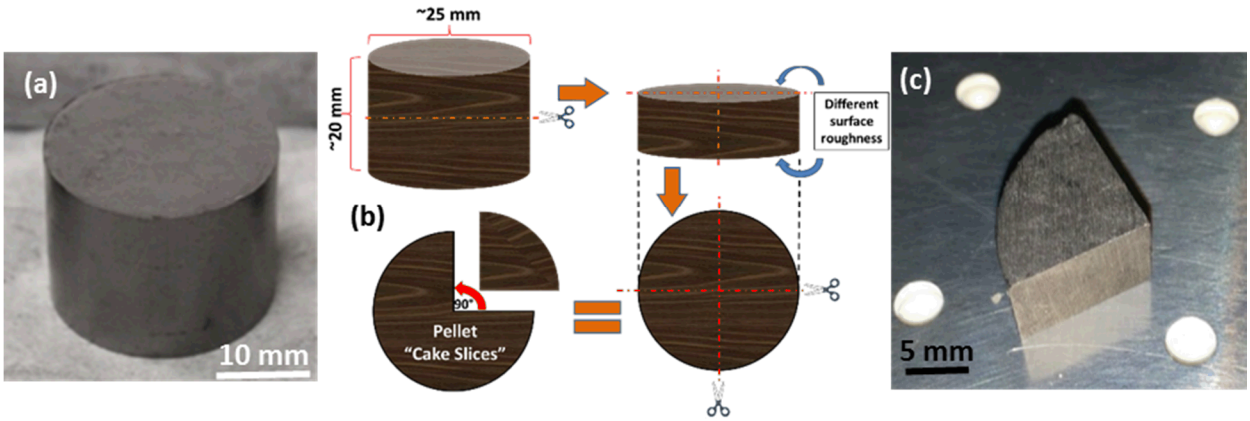

Figure 1. Sectioning of fuel pellet: a) original pellet, b) segmenting diagram and c) “cake slice” sample.

Table 1. Zirconium alloys chemistry.

	Zry-3	Zry-4	Zr-1Nb
Sn, wt.%	0.25	1.412	—
Nb, wt.%	—	—	1.00
Fe, wt.%	0.25	0.2205	—
Cr, wt.%	—	0.1175	—
O, wt.%	—	0.1235	0.138

2.2 X-ray Tomography of Fuel Pellet

A sample was selected for X-ray computed tomography (CT) to evaluate the size distribution of UO_2 particles in the graphite matrix, particle agglomeration, fuel loading percent, and visualize the presence of exposed particles at the pellet surface. The X-ray CT reconstructions were performed using a North Star Imaging (NSI) Micro X-ray Computed Tomography (µXCT) system. A Hamamatsu 150kV micro-focus X-ray tube with a Dexela 2923NDT, Flat Panel X-Ray detector was utilized. The imaging parameters were: 150 kV, 66 µA, a 7 µm nominal spot size, 1080 projections acquired every 0.333°, 178.82° sample rotation, two exposures per projection, resulting in a sample rotation of 178.82°, 9.16 magnification, and an effective pixel pitch of 8.2 µm voxel size.

Figure 2a shows a selected representative radiograph (XY-slice) where UO_2 particles (in white) are contrasted with the black graphite background. The image shows a fairly homogeneous distribution of UO_2 particles in the graphite matrix. The powder is made by standard heat, crush and grind methods. The aspect ratio varies from 1.2 to approximately 3.9 with an average of 1.6. There is no expectation that the slightly elongated nature of the particles will affect any performance metric. Two large Urania agglomerates can be observed in the interior and near the surface of the pellet. It appears that many urania particles are very close or right at the edge of the pellet surface; this could cause physical contact with the clad material and potentially some kind of chemical interaction.

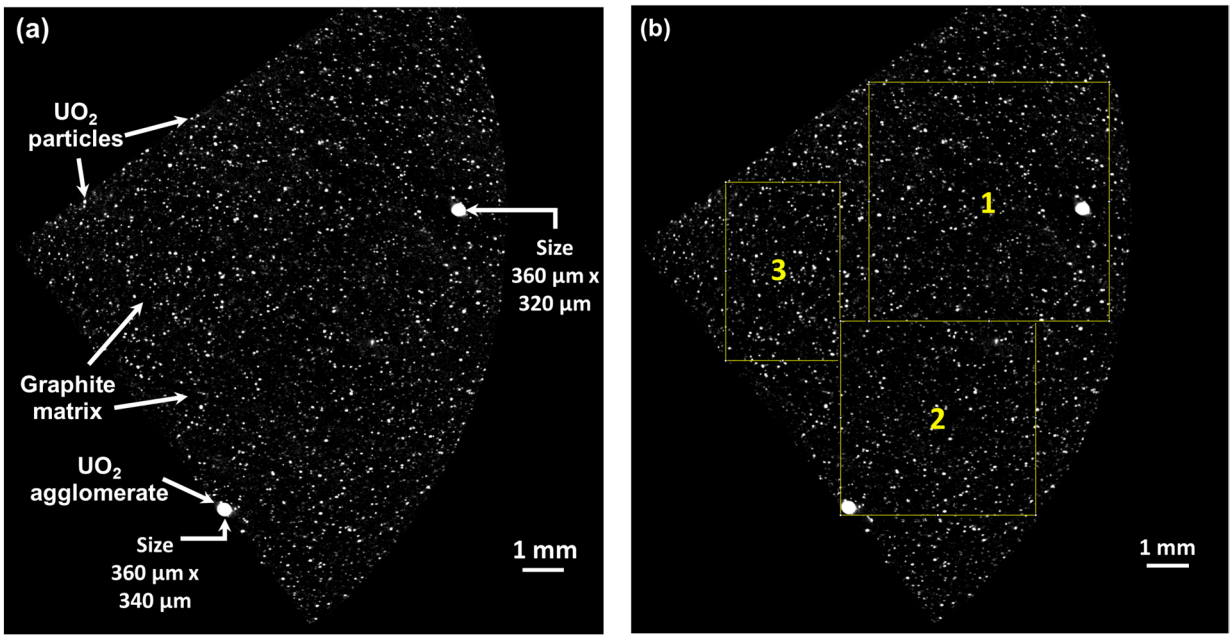

Figure 2. Radiograph: a) UO_2 particles and agglomerates in graphite matrix and b) image analysis areas.

The ImageJ 1.50i software (National Institutes of Health, USA) was used for image processing and analysis of the selected radiograph. The highlighted sections (1-3) in Figure 2b were selected for analysis of UO_2 particles and large agglomerates. The radiograph was processed for statistical analysis. Over a thousand particles were analyzed as ellipses to obtain area and dimensional measurements (major/minor axes length and angle), along with shape descriptors such as circularity ($4\pi \cdot A/p^2$) and inverse aspect ratio (roundness = minor axis/major axis of elliptical particle) of the particles. The average particle equivalent diameter size is 37.6 µm ± 18.7. The shape descriptor analysis confirms the ellipsoidal shape of the particles (circularity factor: 0.962 ± 0.082; roundness factor: 0.754 ± 0.182). The large agglomerates had an equivalent diameter of 342.5 and 355.7 µm, respectively. The UO_2 fuel loading is 2.33%. Figure 3 displays the particle size distribution histogram down to the resolution limit (~8µm). The particle size distribution revolves around ~38 µm and over 85% of the particle population size is within 10-50 µm range, in fair agreement with the reported specification of < 44 µm particle size. It appears that some of the urania particles are very close or right at the edge of the pellet surface.

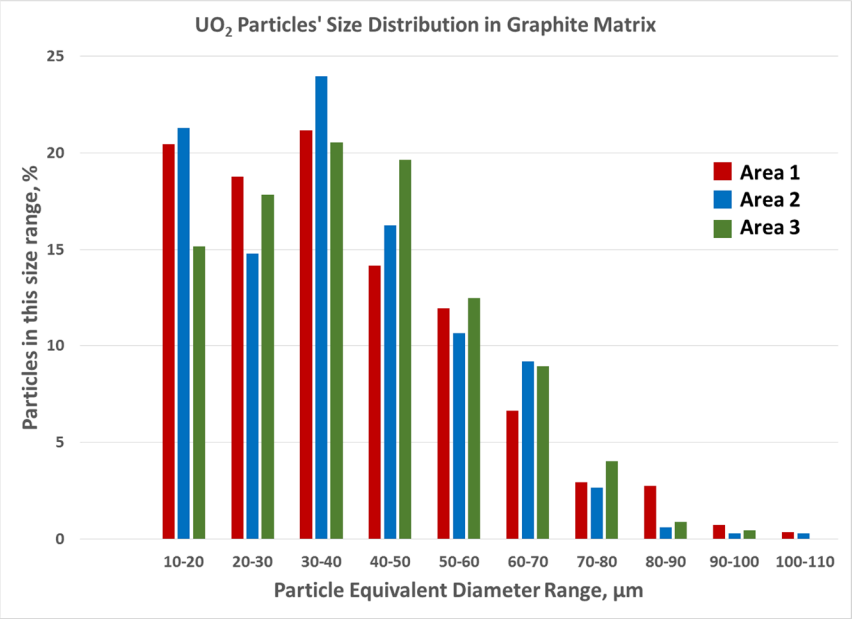

Figure 3. Urania particle size distribution in graphite matrix histogram for selected areas of the pellet.

2.3 Experiment set-up

Though there is limited information on the tests performed and results on the original TREAT HEU U_3O_8 graphite fuel and the Zry-3 clad alloy compatibility, the information available was used to support the experimental design of the interaction tests for this study The test time was of two weeks (or 336 hours) at 820°C (accident scenario temperature) is a conservative estimation and it is significantly longer than the life expectancy of the cladding at 820°C which is only about 20 hours. Even though the temperature profile of the fuel over its lifetime it is not exactly known the experiment was designed to identify potential reactions under extreme conditions [7,8]. The FCCI study was performed on two "cake slice" fuel samples with distinct surface finish (i.e., 150- and 320-grit SiC paper) sandwiched by Zry-4 and Zr-1Nb alloy sheets using a kovar jig at 5.4 N-m torque and sealed inside a quartz capsule at high vacuum (0.6 mPa) as seen in Figure 4a. The two FCCI diffusion couples were placed inside a Thermolyne 79300 ceramic tube furnace, and temperature was increased (20°C/min) up to of 820°C and held for two weeks. As seen in Figure 4b, the glass capsules containing the FCCI assembly are in thermal contact and temperature monitored with a Type K thermocouple. After the two-week anneal, the samples were

furnace-cooled and prepared for post-test analyses. More details on the experimental setup were presented in previous publication [9].

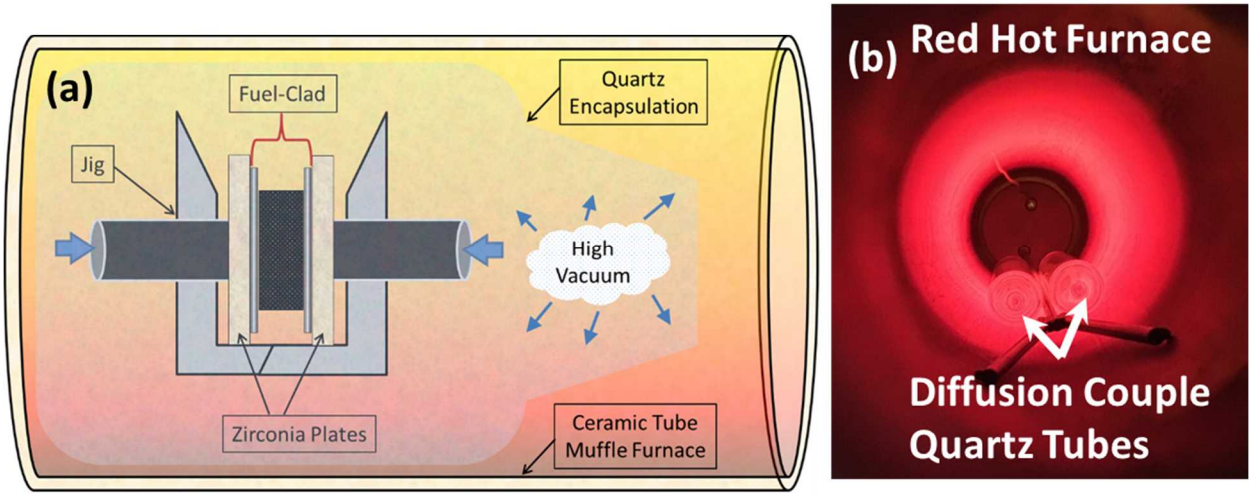

Figure 4. a) FCCI experiment setup and b) view of FCCI samples in furnace.

3. Thermodynamic Modeling Results and Discussion

The thermodynamic modeling was performed with Thermo-Calc 2017b software using the CALPHAD method. Thermodynamic databases utilized: SSUB6 (Thermo-Calc, SGTE substance database, v6), TTZR1 (Thermotech Ltd., Zr-based alloys database, v1) [10] and the U-Pu-O-C database (CEA, TAF-ID v2) [11].

3.1 Composite Fuel Phase Stability in U-O-C System

As previously stated, the TREAT reactor fuel is composed of micron-sized uranium oxide particles homogeneously dispersed in a graphite matrix. Even though the TREAT fuel is technically a composite material, for the thermodynamic modeling we are going to assume this material behaves as an alloy with homogeneously dispersed fine precipitates to acquire some useful information in regards to phase stability and comparison to experimental results. The results should be representative since there is indeed some minor solubility of the constituent elements in each other, and the dispersed particles could be treated as a finely distributed secondary phase in the main phase. In order to analyze the thermodynamic equilibrium of the fuel constituents and equilibrium phases, a series of U-O-C ternary system equilibrium isotherms in the temperature range from 200 to 1,000°C were prepared (Figure 5). The temperature range was selected based on the fuel fabrication outgassing process and reactor operation temperature range (250-950°C). The isopleths denote the stable phases in distinct regions of the diagram delimited by elemental composition as a function of temperature.

The nominal composition (calculated based on the sample constituents) of the pellet used in this study [C=99.74; U=0.08%; O=0.17%] is very similar to the current conceptual design TREAT LEU fuel composition [C=99.87%; U=0.08%; O=0.17%] where the carbon-to-uranium ratio is 1,170 and 2,370, respectively [6]. To easily identify the composition in the U-O-C ternary diagram, a red dot has been placed at the carbon-rich corner of each isopleth presented in Figure 5. The fuel composition lies between two large regions in the equilibrium ternary phase diagram where UO_2+Graphite+CO and UO_2+Graphite+(UC or U_2C_3) are the stable phases. In order to understand if the carbothermic reduction

of UO_2 is energetically favorable, an Ellingham diagram was calculated. Figure 6 displays the thermodynamic viability of the reaction of $UO_2+7C \rightarrow U_2C_3+4CO$ moving forward as a function of temperature and pressure in an inert gaseous environment. Based on previous thermodynamic and U-C phase diagram analysis, the formation of U_2C_3 carbide was emphasized because in the-U-O-C system the formation of U_2C_3 is more energetically favorable from 200-1,000°C and above 99 atomic % C than either UC or UC_2 carbide (UC_2 is stable above 1,400°C) [12]. Figure 6 shows that the Gibbs free energy change (ΔG) of the $UO_2+7C \rightarrow U_2C_3+4CO$ reaction becomes more negative as the pressure is decreased, hence increasing the viability of carbothermic reduction of UO_2 at lower temperatures. A negative value for ΔG indicates that a reaction can proceed spontaneously without external inputs, while a positive value indicates that it will not. This is important for the TREAT element design because the assembly is under vacuum; therefore, the effect of sub-pressure on the reaction must be understood in particular for the Urania particles exposed at the exterior of the fuel block as seen in the tomography (Figure 5).

Based on this analysis, the pressure inside the assembly should preferentially be maintained above 0.6 mPa to restrict carbothermic reduction of urania below 820°C, which is very conservative since the most energetic transient pulse in TREAT is limited to 600°C (fuel peak temperature), and the time at temperature is a few seconds because cooldown takes place immediately after the transient peak.

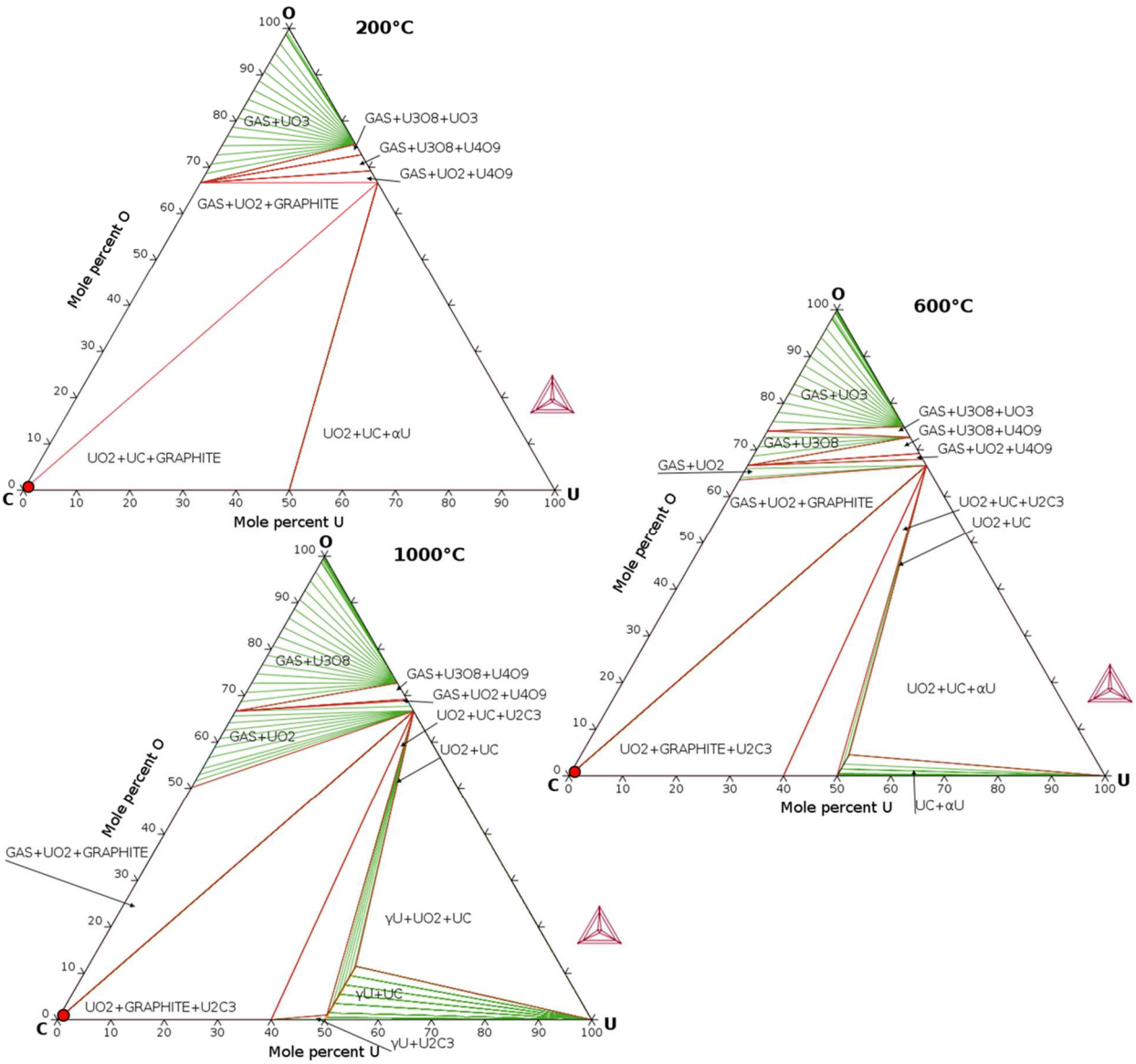

Figure 5. U-O-C isotherms from 200-1,000°C and location of conceptual TREAT LEU fuel composition.

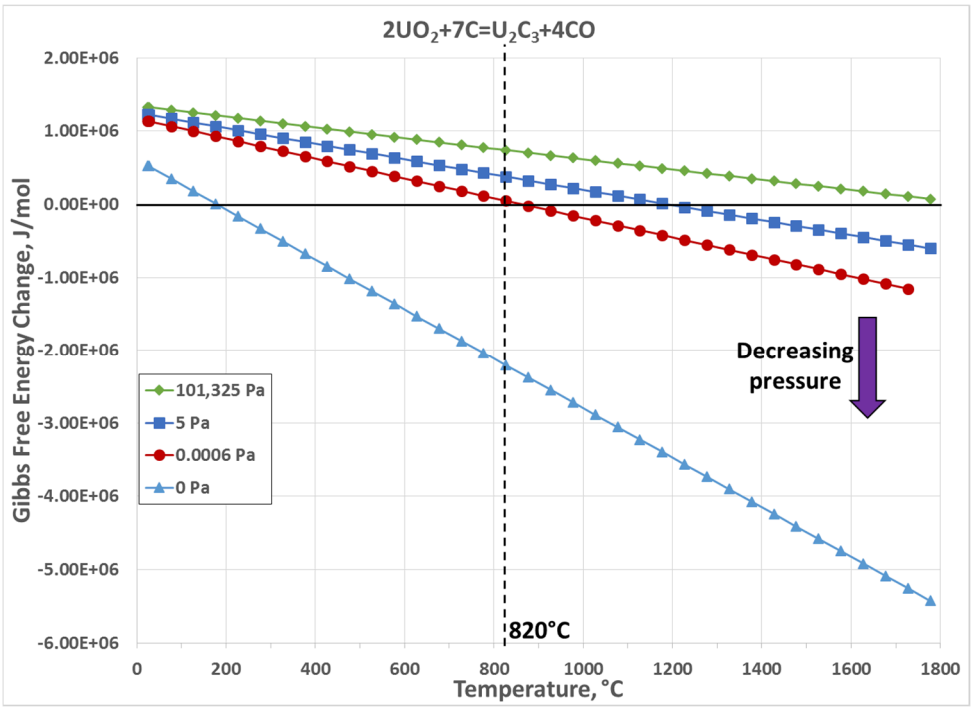

Figure 6. Ellingham diagram of the carbothermic reduction of UO_2 and production of U_2C_3 and CO

3.2 UO_2 + Zr Chemical Stability

Zirconium, like Titanium, is an oxygen scavenger material, and can strip oxygen from other materials at elevated temperature. In order to analyze potential red-ox reactions between UO_2 fuel particles and Zr-alloy cladding, the ΔG of $U+O_2 \rightarrow UO_2$ and $Zr+O_2 \rightarrow ZrO_2$ reactions were modeled and used to determine the relative ease of reducing UO_2 by Zr metal, via the following reaction: $UO_2+Zr \rightarrow U+ZrO_2$ (Figure 7). It is observed that ZrO_2 is energetically more stable (more negative ΔG) than UO_2 at atmospheric pressure, from 25°C to about 1,800°C. As pressure decreases (1 atm = 101,325 Pa→5 Pa→0.6 mPa), the relative slope of the lines shift until they converge at about 1,400°C for a 0.6 mPa vacuum marked as "oxide stability reversal point" in Figure 10.

The analysis shows that the reduction of UO_2 by Zr is possible. However, the reaction kinetics will be rather slow at the low temperature of the reactor normal operation (~280°C) and short period of time at peak temperature (280-600°C) during transient heating. The time at temperature during cooling after the transients (~10 hours cooling to room temperature) should not significantly impact the reduction kinetics either because it has been observed that Zr and its alloys do not oxidize significantly in either air or water below 600°C; therefore, a reaction with oxygen in solid UO_2 should be slower than when compared to oxygen in gaseous or liquid form [13, 14]. For example, even after 35-years of TREAT reactor operation with the original HEU fuel, recent NDE of the cladding via ultrasonic inspection did not show any evidence of localized oxidation, or thinning, of the cladding material beyond the limits specified in the Final Safety Analysis Report. Nonetheless, currently the service time of the HEU core is slightly shorter than the 40-year service life expected for the LEU core.

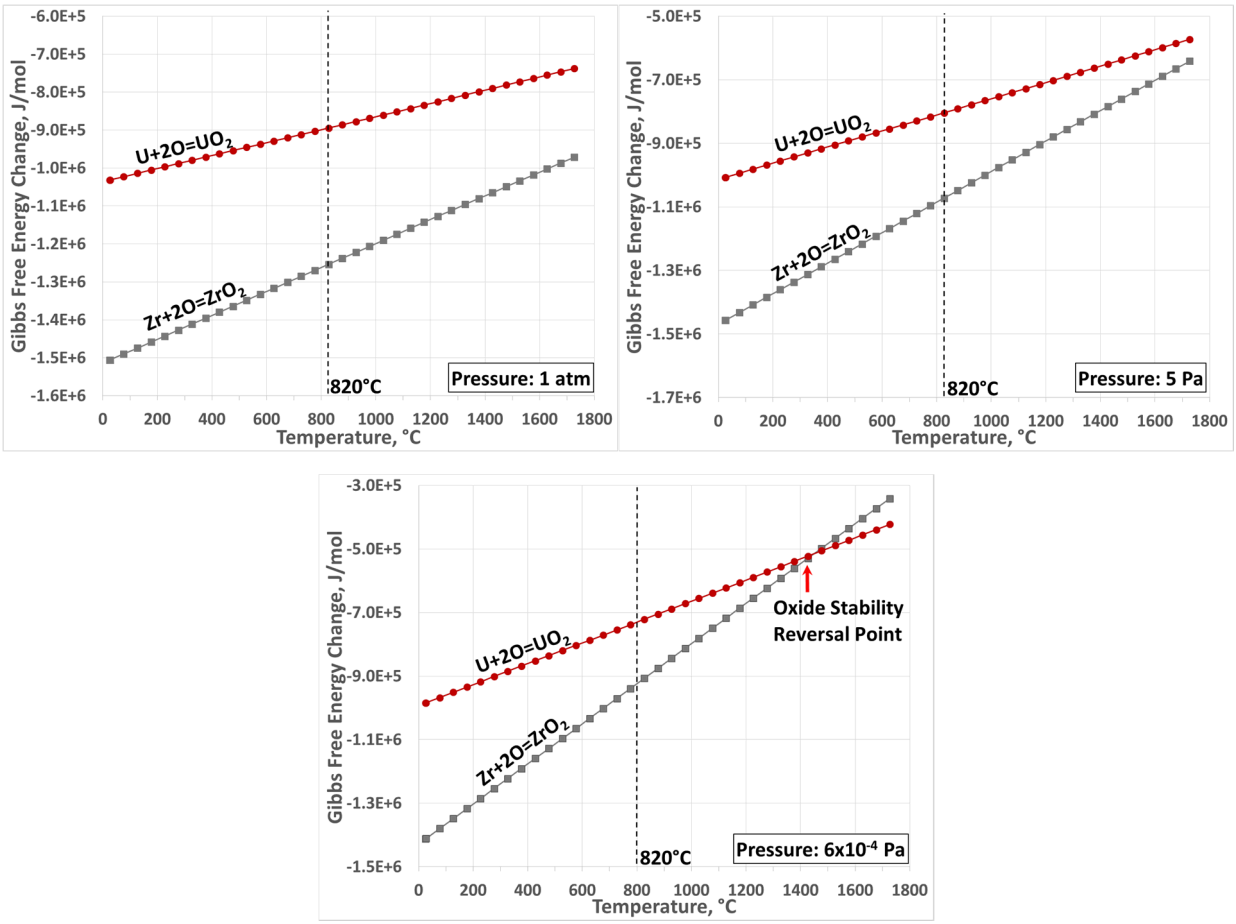

Figure 7. UO_2 and ZrO_2 relative stability as a function of temperature and pressure.

3.3 Effect of Carbon on the Zr-alloys

Thermodynamic modeling was performed to predict the equilibrium phase stability and the effect of carbon on Zircaloy-4 and Zr-1Nb alloys because the predominant elements in this FCCI study are carbon and zirconium. In pure zirconium, carbon has no solid solubility in αZr (<863°C) and approximately 1 at. % in βZr which is only stable above 863°C. Similarly, Zr does not display any solid solubility in graphite. Zirconium monocarbide (ZrC) is the only stable intermediate phase in the Zr-C system; therefore, it can be expected that the interaction of C with Zr will eventually drive the precipitation of ZrC, where the proportion of ZrC will progressively increase as the carbon concentration increases. The equilibrium ZrC composition ranges between 33-50 at.% Carbon with Zr balance [15-17].

Figure 8a-b display the change in proportions of equilibrium phases for Zry-4 and Zr-1Nb alloys (without carbon additions) in the 500°C to 2,900°C temperature range which covers a range beyond the TREAT operation or design basis accident (DBA), but is expanded due to the importance in high temperature nuclear reactor severe accident environments where the UO_2 fuel can reach temperatures over 2,800°C and melt. In Figure 8a, it is observed that below 800°C the main phase (>90%) in Zry-4 is αZr with small proportions of Zr_7FeSn_2 and Zr_3Fe secondary phases formed by the alloying elements. In the range of 800°C to 930°C the material experiences the progressive transformation of αZr into βZr as temperature increases, and the formation of a solid solution of βZr phase. Upon heating, it starts melting at the solidus temperature (1,690°C) until it melts completely at the liquidus temperature (1,820°C). Similarly,

Figure 8b shows that below 627°C the Zr-1Nb alloy displays a matrix of αZr phase with a small proportion (<0.6%) of βNb phase in equilibrium. As temperature increases, the Zr-1Nb alloy goes through the α→β transformation in the temperature range of 627°C to 916°C. As the microstructure transforms into the HCP structure, the alloying elements go into solution in the high temperature βZr phase. βZr is stable in the 916°C to 1,827°C, then rapidly melts above 1,827°C. Furthermore, the effect of 1 weight % carbon concentration in both Zry-4 and Zr-1Nb is displayed in Figure 8c-d. It is remarkable that, with just 1 wt.% carbon addition in the Zr-alloys, about 20% of Zr is exhausted for the formation of ZrC phase. The ZrC is a highly refractory material (melting temperature: 3,540°C) and according to the thermodynamic modeling, it will remain solid in the microstructure up to about 2,500°C. This value is somewhat inferior to the experimentally determined ZrC-C eutectic point corresponding to 2,927°C [15-17]. Figure 8e-f displays the increment in ZrC phase as a function of increased carbon concentration (0.01 to 1 wt.%) on Zry-4 and Zr-1Nb. The proportion of the secondary phases in Zry-4 (i.e., Zr_7FeSn_2 and Zr_3Fe) and Zr-1Nb (i.e., βNb) do not seem to be affected by the ZrC formation; this means that the alloying elements do not seem to interact with carbon in the Zr-matrix.

The previous thermodynamic analysis predicts that in the range of the TREAT reactor operation [280-600°C] and DBA [820°C] temperature, carbon will preferentially interact with Zr to form zirconium carbide with the Zr-alloys presented in this study.

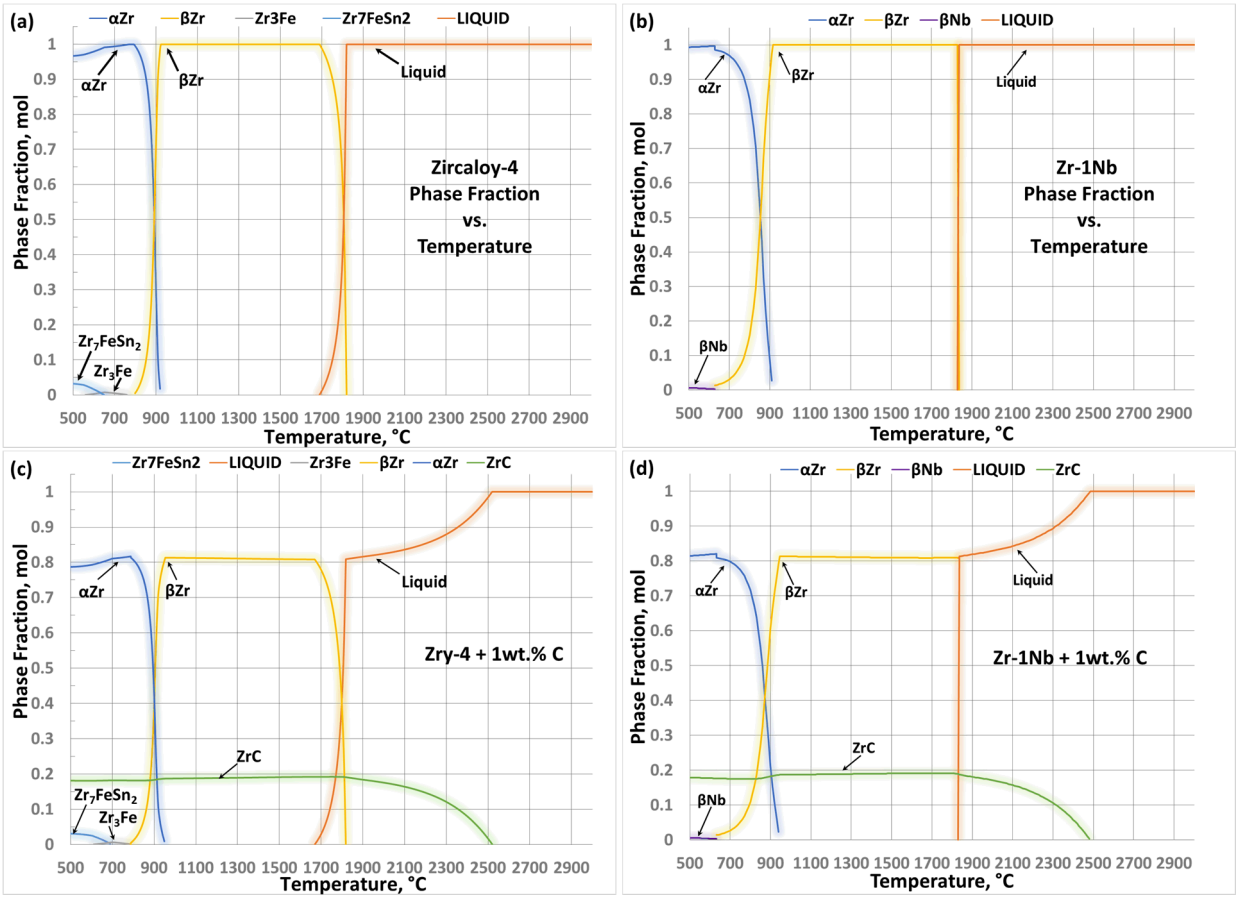

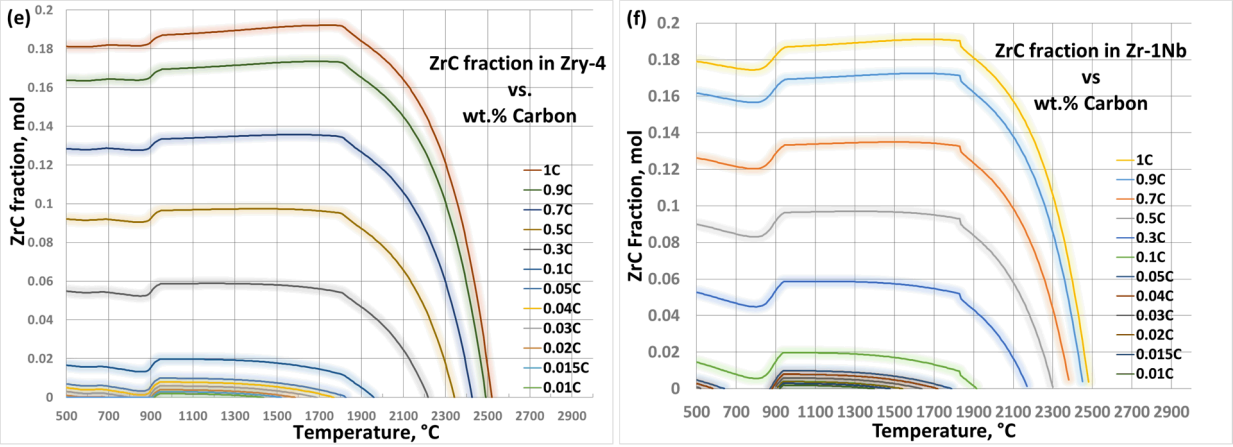

Figure 8. Calculated change in ZrC phase fraction in Zry-4 and Zr-1Nb alloys as a function of temperature and carbon concentration.

4. Experiment Results and Discussion

This section provides the analyses performed on the fuel-clad diffusion couples after a 336-hour anneal at 820°C under vacuum 0.6 mPa. The temperature and pressure were selected as bounding conditions to represent the RIA scenario in TREAT reactor, and the high vacuum utilized during electron beam welding. E-beam welding is currently in consideration as a potential welding method to seal the fuel assembly.

4.1 Physical Appearance of Fuel-Clad Diffusion Couple after FCCI test

The glass capsules were visually inspected after completion of 336 hours FCCI annealing and furnace cooling. Upon visual inspection (Figure 9), a dark tarnish is noticeable on the Zr-alloy metallic sheets, including the zirconia ceramic pieces, possibly from CO or other carbonaceous gases that might have evolved from the fuel pellet during the test and subsequently interacted with the Zr-based materials. CO gas may be generated during carbothermic reduction of UO_2 or from the outgassing of trace quantities of organic resins that were not successfully evolved during the post-fabrication treatment of the pellet. There is no apparent discoloration or staining on the Kovar jig or the quartz glass capsule walls, providing an indication that the reactions were mainly restricted to the central region of the diffusion couple containing the fuel-clad assembly. Subsequent mass spectrometry analyses of non-fueled blocks have shown that the outgassing process used for this pellet did not completely remove all the organic volatiles from the graphite. It is believed that the lower temperature volatiles may have deposited on the Zr-alloy and zirconia material during cooling.

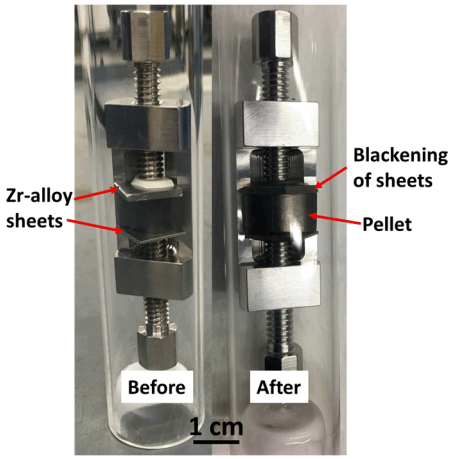

Figure 9. Appearance of the fuel-clad diffusion couple before and after the 2-week annealing at 820°C.

4.2 Sample Preparation for Characterization

To ensure that the diffusion couple and reaction zones stayed intact, the interior of the capsule (after the seal was broken) was filled with a transparent epoxy resin until the diffusion couple was completely immersed. The resin was allowed to harden overnight before cutting operations. After resin hardening, the central part of the diffusion couple was separated from the rest of the jig using a SiC disc on an Accutom-50 Struers High-speed saw. Subsequently, a Buehler IsoMet low-speed saw was utilized with a diamond disc to dissect through the axis of the jig to expose the cross sections of the fuel-clad interface (Figure 10). The semi-cylindrical sections were placed in a cylindrical plastic mold, immersed in epoxy resin, and allowed to harden for ease of fitting in standard fixtures used in the grinding and polishing operations. The samples were ground on an automated turntable using SiC paper (320, 600, 800, 1200 grit), and polished with an aqueous suspension of fine diamond particles (3, 1, and 0.25 μm) on a soft cloth.

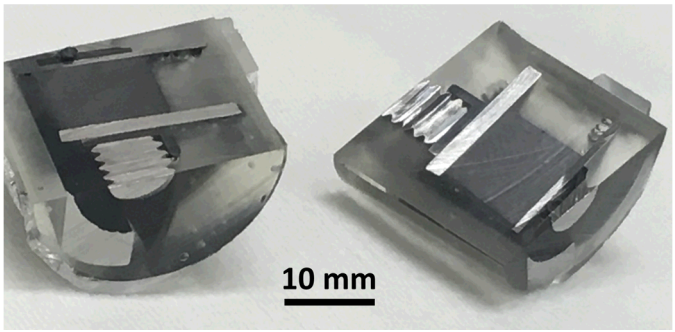

Figure 10. Appearance of fuel pellet-clad sheet diffusion couple after sectioning.

4.3 Interaction Layer Size

Microscopic analysis was performed at the fuel-clad interface to measure the size of the interaction layer. Over 200 measurements were performed, and the summary of the results are presented in Table 2. Although only one sample of each condition was tested and evaluated, results show a potential trend. Analysis shows that the extent of the interaction layer in Zry-4 is the same, regardless of pellet surface finish. The interaction layer observed on the Zr-1Nb sheet shows a dependence on surface finish; for example, it shows a relatively more pronounced interaction layer (twice the thickness) on the sample in contact with the smooth fuel pellet surface (320-grit SiC paper finish) when compared to the sheet surface in contact with the rougher pellet face (150-grit SiC paper finish). Zry-4 sheet does not show a pellet

surface roughness influence on the interaction layer thickness; however, the variability in the interaction layer thickness is higher than that observed for Zr-1Nb, based on the standard deviation calculation and observations. Based on the layer thickness and time at temperature, an interaction rate was calculated.

The previous analysis shows that the FCCI will not be significant, which reduces the possibility of any deleterious effect on the cladding.

Table 2. Roughness measurements.

Alloy Sheet	Fuel Pellet Finish (SiC grinding paper grade)	Interaction Layer, μm	Linear Diffusion Rate at 820°C, nm/hour
Zry-4	320-grit	5.7 μm SD 2.0	~17 nm/h
	150-grit	5.8 μm SD 2.2	~17 nm/h
Zr-1Nb	320-grit	5.7 μm SD 1.2	~17 nm/h
	150-grit	3.1 μm SD 1.0	~9 nm/h

4.4 SEM and XRD Characterization of the Fuel-Clad Interaction Area

In order to evaluate the inter-diffusion, microstructure, morphology and phase formation characteristics at the fuel-clad interaction interface, the experimental study includes SEM in SE and BSE imaging modes along with elemental analysis using energy dispersive spectroscopy (EDS) via line scan and spot/area analyses modes. In addition, an X-ray diffraction analysis was performed to support the crystal structure identification of the main phases at the interaction area. A JEOL JSM-6610 LV (low-vacuum chamber) SEM, with a 10-kV accelerating voltage and a working distance of 10 mm, was utilized in conjunction with an EDAX detector for chemical analysis. The EDS detector was calibrated with a molybdenum sample before analyses. A Rigaku XRD machine with a Cu K_α (λ = 1.540562 Å) X-ray source was used over a 5 to 90° scan range (2θ) with 0.2° step increments.

4.4.1 Zircaloy-4 Sheet and Fuel Pellet Interaction

The main features of interest, e.g., Zry-4 sheet, fuel pellet, interaction area and respective constituent phases, in the FCCI region of the Zry-4 diffusion couple are displayed in Figure 11b. Figure 11a shows a micrograph displaying the characteristic morphology of the interaction layer observed at the Zircaloy-4 – LEU pellet interface on both 320- and 150-grit finish pellet (Figure 11 and Figure 12). The interaction zone of the Zry-4 sheet displays the formation and growth of the zirconium monocarbide phase. The carbide seems to grow outward on the surface of the sheet as opposed to internal carbiding of Zr alloy. This agrees with the fact that there is no solubility of C in Zr as previously stated in Section 3.3. Figure 8b displays the BSE image of the FCCI zone showing a very clear contrast between the cladding, interaction layer, and pellet. Figure 8b also displays the EDS line scan (pink line) across FCCI layer. The plot highlights the change in composition across the Fuel-Clad interaction layer (about 7.5 μm thick). The change in composition corresponding to two precipitates of Zr_3(Fe,Cr) in the αZr-matrix can also be observed in the line scan. Furthermore, Figure 8c displays an electrograph in SE mode where the coral-like morphology of the ZrC can be clearly appreciated. It appears that the carbon attacks the Zr and causes a volumetric expansion as the ZrC grows that tends to separate other regions of the FCCI interface. This results in ZrC precipitation and growth taking place only at locations where the carbide initially formed. Hence, the kinetics of carbide layer growth seem to be controlled by the diffusion rate of C through the ZrC phase [18]. Furthermore in Figure 11c, the measured composition of the ZrC phase shows a slightly carbon-rich stoichiometry with a relatively higher concentration of Fe/Cr and lower Sn than the Zry-4 base material (see Table 1), this means that Carbon preferential reacts with Zr, Fe and Cr.

Even though the EDS is a semi-quantitative analysis at best, it gives an adequate indication of the elements interacting at the fuel-clad interface.

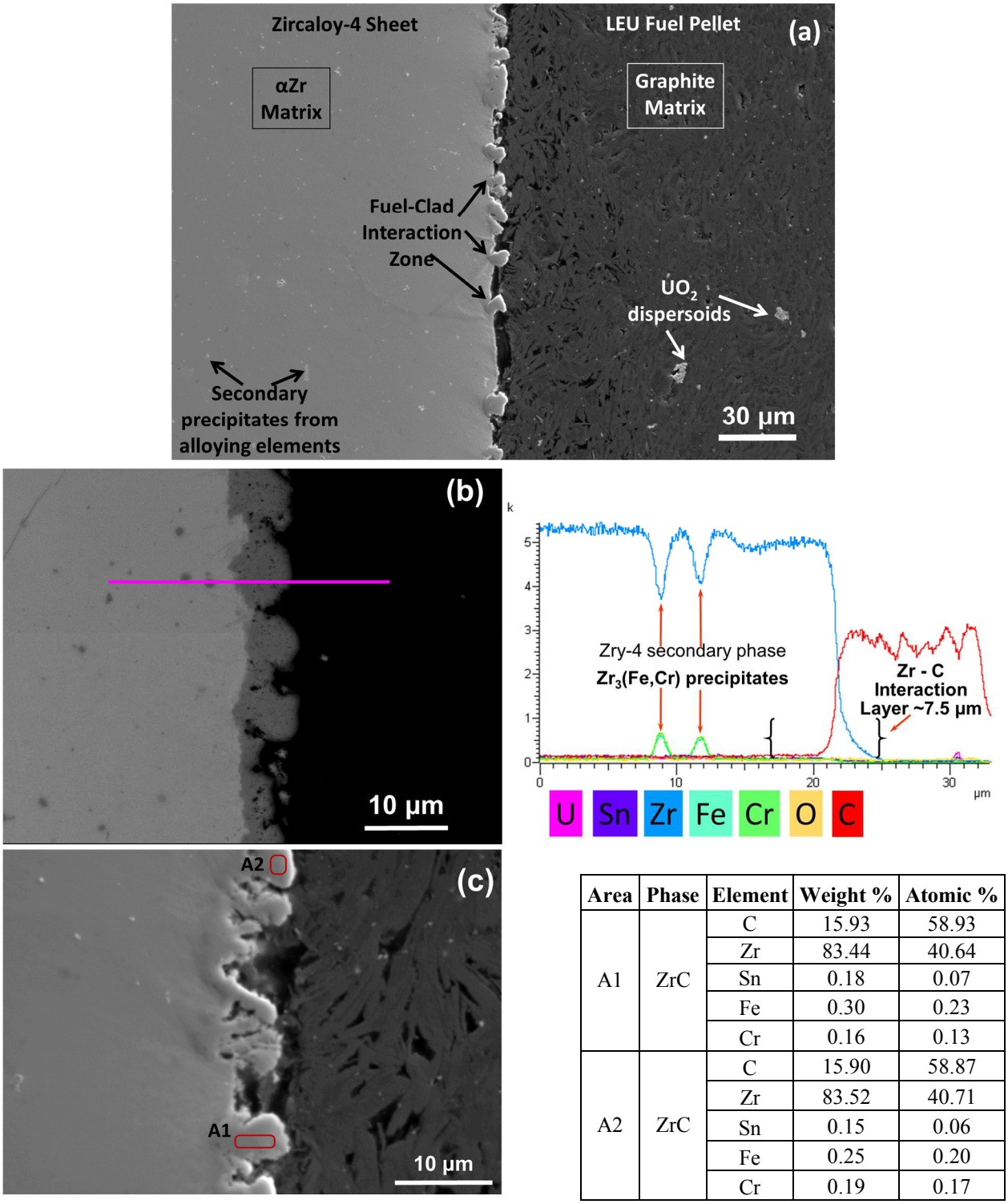

Area	Phase	Element	Weight %	Atomic %
A1	ZrC	C	15.93	58.93
		Zr	83.44	40.64
		Sn	0.18	0.07
		Fe	0.30	0.23
		Cr	0.16	0.13
A2	ZrC	C	15.90	58.87
		Zr	83.52	40.71
		Sn	0.15	0.06
		Fe	0.25	0.20
		Cr	0.19	0.17

Figure 11. a) ZrC formation at fuel-clad interface of Zry-4 sheet (320-grit pellet finish). b) BSE image with EDS line scan and c) SE image with spot analysis of element concentration.

Furthermore, Figure 12 displays part of the microscopic analysis performed along the interaction layer of the Zry-4 sheet in contact with the fuel pellet with relatively rougher surface finish (150-grit). The morphology of the interaction layer is essentially the same as the one observed for 320-grit sample; however, the fuel-clad reaction areas are more separated because of the more irregular contact surface. Figure 12 shows the elemental analysis of the coral-like carbide structure that formed at the fuel-clad interface. It is observed that the composition again corresponds to ZrC with some dissolved iron and chromium, but depleted in tin. An EDS analysis of the Zry-4 base material is also presented where the compositions closely match the chemical analysis in Table 1, showing no change in composition in the base material.

Area	Phase	Element	Weight %	Atomic %
S1	ZrC	C	12.57	52.11
		Zr	86.76	47.35
		Sn	0.19	0.08
		Fe	0.26	0.23
		Cr	0.24	0.22
S2	ZrC	C	13.16	53.44
		Zr	86.30	46.13
		Sn	0.10	0.04
		Fe	0.29	0.25
		Cr	0.14	0.13
S3	ZrC	C	14.87	56.95
		Zr	84.52	42.63
		Sn	0.18	0.08
		Fe	0.27	0.21
		Cr	0.15	0.13
A1	Zry-4	Zr	98.19	98.13
		Sn	1.31	1.00
		Fe	0.31	0.51
		Cr	0.20	0.35
A2	Zry-4	Zr	97.68	97.05
		Sn	1.18	0.90
		Fe	0.59	0.96
		Cr	0.42	0.75

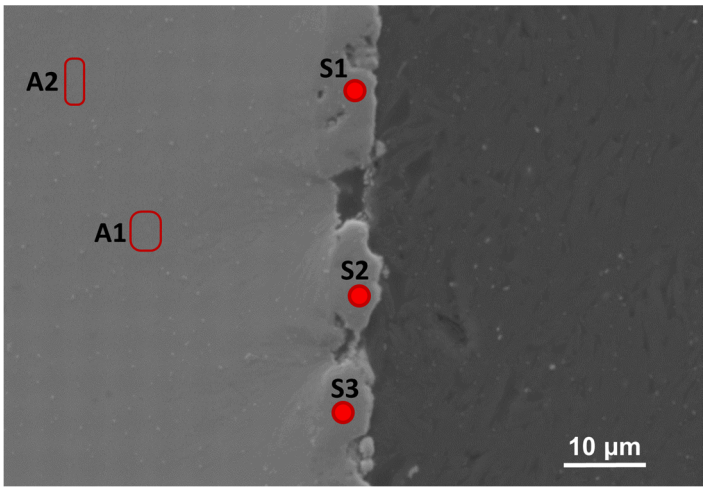

Figure 12. Zirconium carbide (ZrC) formation at clad-pellet interaction layer (150-grit pellet finish) and EDS elemental analysis of metallic sheet and ZrC phase.

As observed in Figure 13, the zirconium depletion via reaction with graphite at the fuel-clad interface promoted the formation of an intermediate phase, expressly Zr_7FeSn_2. This was observed on both Zry-4 samples regardless of the pellet finish and, at many places, along the interaction area. Figure 13a-b show the formation of Zr_7FeSn_2 at the limit between the fuel-clad area and the Zry-4 alloy shown as "white phase" under the BSE imaging mode. The EDS line scan displayed on Figure 13a shows a marked deflection in the Zr plot intensity, or concentration, right after the interaction zone with a respective increase in the concentration of Sn and Fe. According to the elemental analysis presented in Figure 13b, the white phase composition closely matches the stoichiometry of the Zr_7FeSn_2. The formation of the Zr_7FeSn_2 phase was previously predicted in the thermodynamic modeling presented in Section 3.3. However, this phase is normally homogeneously distributed in the Zry-4 alloy through a thermomechanical process to impart improved mechanical strength and creep resistance to the alloy. However, it is clearly observed that the reaction of the Zircaloy-4 alloy with graphite promotes the segregation of the alloying elements, in particular Sn-Fe enrichment, and formation of a continuous intermetallic phase, seen as a "white lining" of Zr_7FeSn_2. Intermetallic phases commonly demonstrate low toughness and a brittle behavior, hence, this could act as a crack initiation site under high bending stress, high strain-rate, or sudden mechanical impact. The zirconium carbide observed in higher concentrations than the Zr_7FeSn_2 is a ceramic with relatively lower fracture toughness compared to metals. However, the stress level in the cladding is nominally zero. The

cladding must support its own weight in service. During fuel loading and unloading, additional stress may be applied; however, calculations indicate that a cladding thickness of only 0.002-inch is sufficient to allow successful extraction of the fuel element. A safety factor of 5 is used therefore and a 0.010-inch cladding thickness is required for operation.

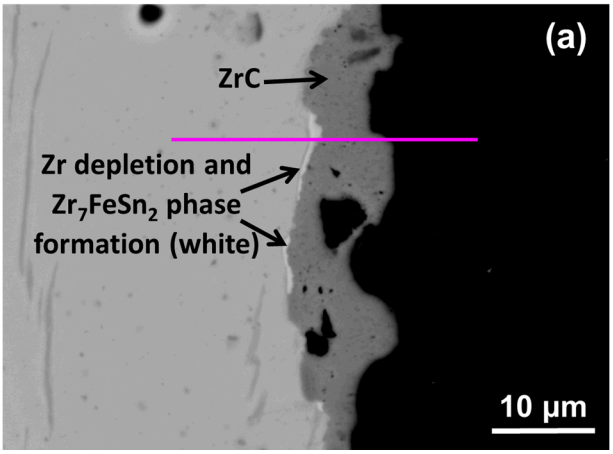

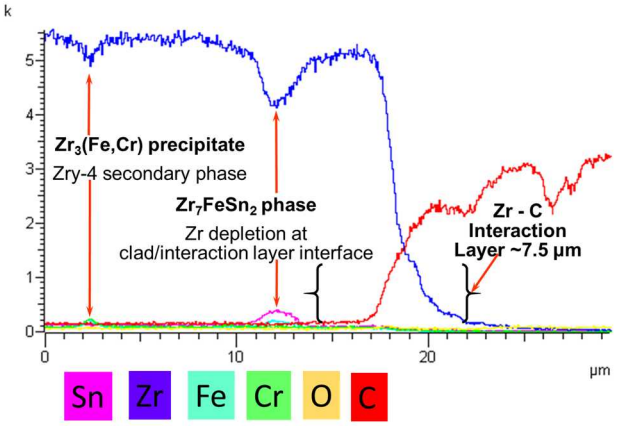

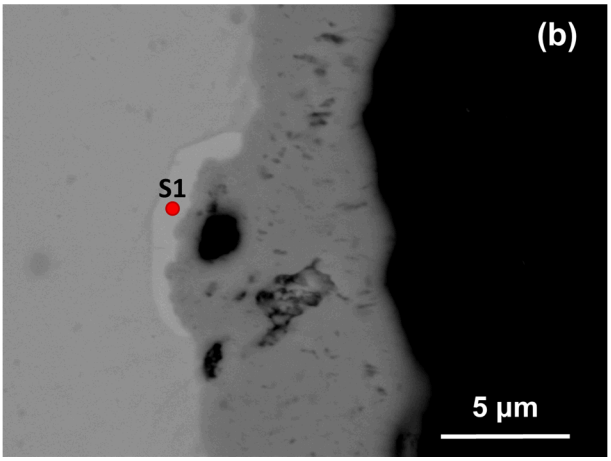

Area	Phase	Element	Weight %	Atomic %
S1	Zr_7FeSn_2	Zr	80.76	81.52
		Sn	15.21	11.80
		Fe	3.96	6.53
		Cr	0.08	0.14

Figure 13. a) Micrograph and graphical presentation of elemental analysis using EDS line scan showing Zr depletion and formation of Zr_7FeSn_2 phase at b) sheet side of interaction layer.

Finally, in order to corroborate the formation of ZrC at the fuel-clad interaction layer, XRD analysis was performed at three areas along the Zircaloy-4 sheet-fuel pellet interface. Figure 14 presents representative XRD patterns from the FCCI zone for the 320-grit and 150-grit pellet finish in contact with the Zircaloy-4 sheet. The XRD scan helped to confirm the formation of ZrC with cubic crystal structure on both samples. Similarly graphite, zirconium (HCP lattice), UO_2 and residues of monoclinic ZrO_2 (expected due to the ease of Zr oxidation and native oxide formation) are included in the XRD scan. The corresponding powder XRD database cards utilized for the peak detection and fitting are: ZrC (01-074-1221), graphite (00-056-0159), UO_2 (01-071-6416), αZr (01-078-2921) and ZrO_2 (01-079-1764).

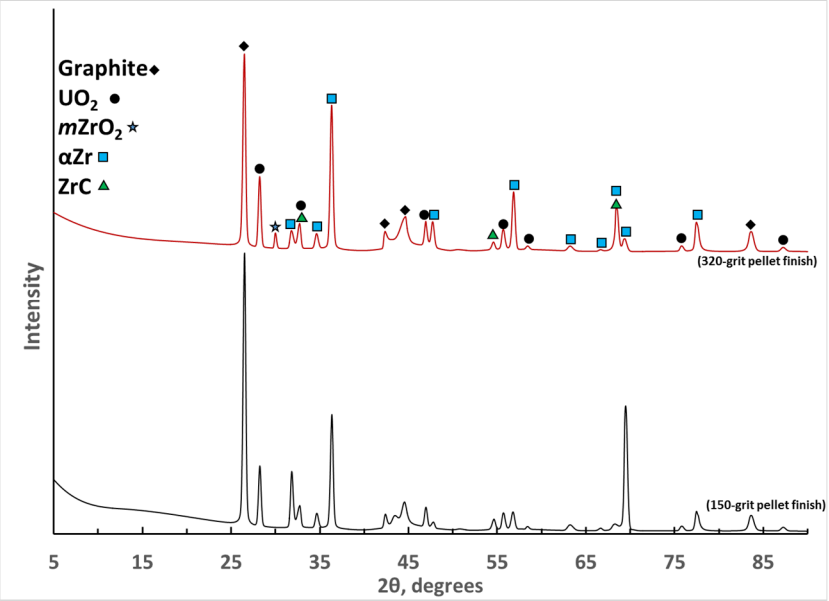

Figure 14. X-ray diffraction scan of Zry-4 sheet - fuel area (320- and 150-grit pellet finish).

4.4.2 Zr-1Nb Sheet and Fuel Pellet Interaction

This section displays the characterization and analysis of the FCCI interface between the fuel pellet and Zr-1Nb sheet. Figure 15a displays a micrograph depicting the main areas of interest corresponding to the cladding sheet, the fuel pellet and intermediate reaction zone, respectively, and the constituent's phases of clad and fuel. Figure 15a displays a discontinuous interaction layer at the clad-fuel (320-grit finish interface). It shares similarities with the carburization layer observed on the Zry-4 alloy, but the ZrC phase is more rounded. Figure 15b and Figure 15c show a BSE and SE image, respectively, where the interaction layer is observed. An EDS line scan (pink line) across the pellet-clad is accompanied by a plot (right) of selected elements' (Zr, Nb, C, U and O) X-ray signal intensity as a function of distance. The discontinuous interaction zone is about 6 µm and 4 µm for the 320- and 150-grit fuel pellet finish, respectively, falling within the variability of the measurements presented in Table 2. Figure 15b shows higher concentration of Nb (white) at the grain boundaries denoted in the line scan plot as a depression in the Zr and increase in Nb signal at the grain boundary.

Electron microscopy observations at the fuel-clad interaction of both Zry-4 and Zr-1Nb alloys show distinct areas where the ZrC has a relatively rougher or smoother morphology. It was observed that a more intimate contact between cladding and fuel promoted more growth of the ZrC local structure in comparison to other sections where there was a relatively a poorer physical contact or not as tight fit. It is also important to mention that even though this is an out-of-pile test the relatively low fuel burn-up expected for the TREAT reactor operation is considered to have negligible radiation damage effects and impact on the growth of the ZrC at the cladding-fuel interface.

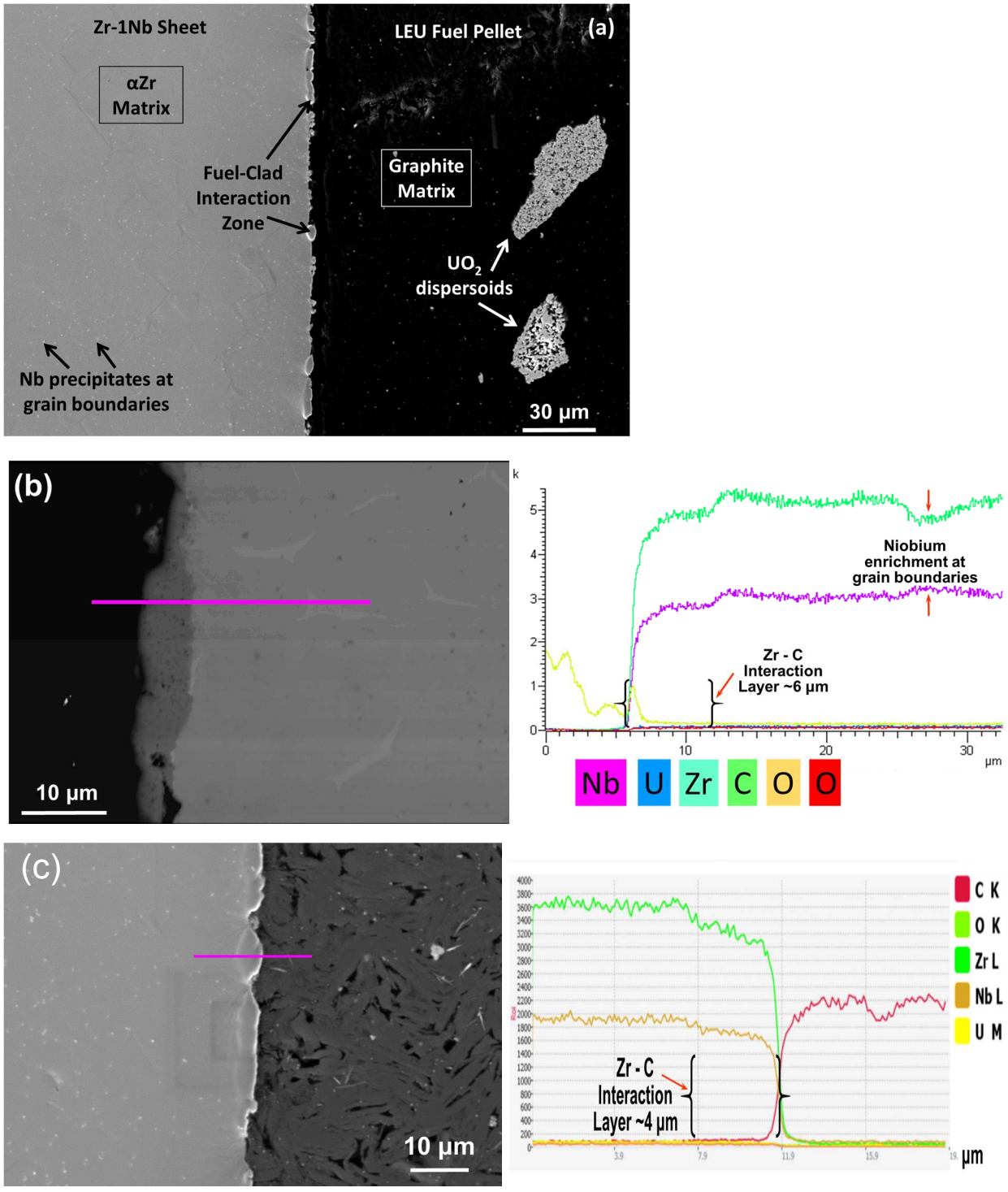

Figure 15. a) Zr-1Nb sheet carburization zone and ZrC formation with fuel pellet (320-grit finish). b) EDS line scan across interaction area. SE and BSE imaging mode (b) 320- and c) 150-grit pellet finish.

Figure 16 displays the areas where elemental analysis sampling was performed. The carbided layer shows a carbon-rich ZrC with dissolved Nb concentration corresponding to the proportion observed in Zr-1Nb base material. This indicates that Nb is not segregating to the edge of the interaction area as observed for

the alloying elements in Zry-4 alloy. The EDS analysis on the clad sheet closely resembles the element concentration displayed in Table 1, showing no change in composition of the alloy.

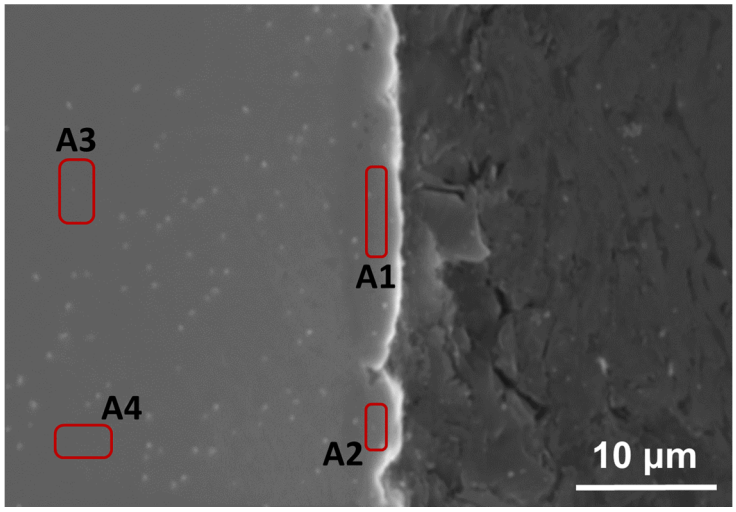

Area	Phase	Element	Weight %	Atomic %
A1	ZrC	C	16.22	59.52
		Zr	82.57	39.91
		Nb	1.20	0.57
A2	ZrC	C	17.64	61.93
		Zr	81.18	37.53
		Nb	1.18	0.53
A3	Zr-1Nb	Zr	99.09	99.10
		Nb	0.91	0.91
A4	Zr-1Nb	Zr	98.66	98.70
		Nb	1.33	1.31

Figure 16. Elemental analysis of carburization zone and base Zr-1Nb alloy sheet (320-git pellet finish).

Two sets of three XRD scans were performed along the Zr-1Nb sheet and fuel pellet interface for phase identification. Figure 17 displays the XRD pattern for both the 320-grit and 150-grit finish pellet surface in contact with the cladding material. The XRD scan confirmed the presence of cubic ZrC phase and also displays the αZr matrix and secondary phase BCC-Nb (XRD card: 00-035-0789) along with the fuel graphite matrix and UO_2 ceramic distinctive diffraction peaks. No unexpected peaks were found.

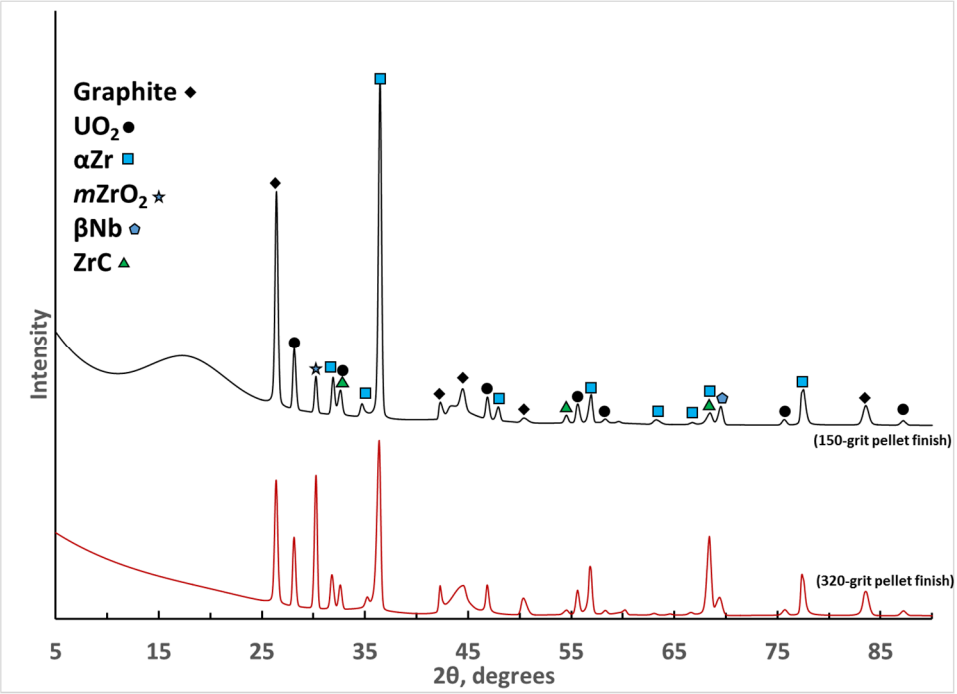

Figure 17. X-ray diffraction patterns of Zr-1Nb sheet - fuel area (320- and 150-grit pellet finish in red and black respectively).

5. Conclusions

The 336-hour FCCI diffusion couple test at 820°C under high vacuum (0.6 mPa) resulted in the carbiding of both the Zry-4 and Zr-1Nb alloy sheets by the fuel pellet. The interaction between graphite fuel composite and Zr-alloy cladding resulted in the formation of a discontinuous zirconium carbide layer. For the Zry-4 sheet, the FCCI interaction layer thickness and non-uniformity (standard deviation) measured is very similar regardless of the pellet surface finish (150-grit vs. 320-grit sanding paper ground finish). Zr-1Nb alloy FCCI layer thickness shows some influence of the pellet surface finish on the interaction, where the size of the interaction layer thickness doubles at the smooth pellet finish (320-grit pellet finish) when compared to the rougher surface finish (150-grit pellet finish). Formation of a Zr_7FeSn_2 intermetallic region was identified for the Zry-4 experiment due to the exhaustion of Zr at the fuel-clad interface and segregation of alloying elements at the limit of the interaction zone. On the other hand, Zr-1Nb does not show segregation of Nb nor the formation of other secondary phases outside the interaction area caused by the carbiding. Visual inspection of the exposed Zr-alloy sheet exposed surface shows a tarnish soot-like layer, indicating that some carbonaceous material deposited on the surface. This indicates that a carbon containing gas evolved during the isothermal test and later plated on the Zr-alloy sheets. The source of the gas could be either a result of incomplete outgassing of organic resin residues from fuel pellet fabrication, or production of CO from the carbothermic reduction of UO_2 favored at lower vacuum. The interaction between Zr and UO_2 could not be confirmed because no particles were found in physical contact with the sheet at the cross-section analyzed. On the other hand, the carbiding process of the Zr-alloy cladding and preferential formation of ZrC at the FCCI layer was well predicted by the thermodynamic modeling.

In summary, the extent of the reaction between the conceptual TREAT LEU fuel and both the Zry-4 and Zr-1Nb clad materials is minimal and results in an interaction layer in the range of 3-6 μm after a 336-hour exposure at 820°C. The fuel-clad interaction experiment gives insight on the viability of utilizing either of the nuclear-grade Zr-alloys in this study. However, the Zr-1Nb alloy seems to have a slight advantage over the Zry-4 alloy performance because a) Zr-1Nb shows less interaction with the graphite matrix of the fuel, b) no alloying element segregation was observed, and c) Zry-4 forms an intermetallic phase region at the fuel-clad interface that could pose some disadvantages due to the inherent brittleness of this type of intermediate phase. This study compared the FCCI for Zry-4 and Zr-1Nb alloys. It is recommended that a complementary study be performed on Zry-3 FCCI in order to distinguish if similar reactions would take place at the fuel-clad interface.

6. Acknowledgements

This work has been performed under the auspices and support of DOE NNSA. Our gratitude is extended to Karen Wendt and Rob Seifert for the computer tomography acquisition; Russell Lewis for glass blowing operations for fabrication of quartz capsule components; Tim Smoley for machine shop support for kovar jig fabrication; Michael Benson for test and glass encapsulation operation support; Joe Palmer for supplying zirconia ceramic plates; Dr. Chao Jiang for providing the U-Pu-O-C thermodynamic database; and Jatu Burns, Allyssa Bateman, Dr. Lingfeng He and Bryan Forsmann for XRD, SEM, and sample preparation support.

7. References

[1] Zinkle, S. J., Terrani, K. A., Gehin, J. C., and Ott, L. J. "Accident tolerant fuels for LWRs: A perspective," *J. Nucl. Mater.* 448, 2014, 374–379.
[2] Lyons, P. B. "Resumption of Transient Testing of Nuclear Fuels Project Approval of Critical Decision (CD) 0," Approved Mission Need, PBL-12-2-2010, 2010.

[3] van Rooyen, I. J., Morrell, S. R., Jamison, R. K., Crawford, A. L., Hartman III, H. T., Luther, E. P., Wright, A. E., Kontogeogakos, D. C., , Papadias, D. D. Connaway, H. M., and Yesilyurt, G. "Performance and Fabrication Status of TREAT LEU Conversion Conceptual Design Concepts," Proceedings, *RERTR-35th International Meeting,* 2014, CON14-33130.
[4] Freund, G. A., Iskenderian, H. P., and Okrent, D. "TREAT, a Pulsed Graphite-moderated Reactor for Kinetic Experiments," P/1848, Session B-12, U.S. Government Printing Office, 1958, 461–475.
[5] van Rooyen, I. J., Woolstenhulme, N. E., Jamison, R. K., Luther, E. P., Valenti, L. N. "TREAT Conversion LEU Fuel Design Trade Study", INL/LTD-14-31704 Rev. 1, November 2015, 49-56.
[6] Connaway, H. M., Kontogeorgakos, D. C., Papadias, D. D., Brunett, A. J., Mo, K., Strons, P. S., Fei, T., and Wright, A. E. "Analysis of the TREAT LEU Conceptual Design" Pub. SciTech Connect, RTR/TM-16/1, Argonne National Laboratory, Nuclear Engineering Division, 2016, 1-74.
[7] Foote, F. G., Schumar, J. F., and Chiswik, H. H. "ANL-5797: Quarterly Report", Argonne National Laboratory, Metallurgy Division, AEC R&D Report, October 1958, 22-23.
[8] Freund, G. A., MacFarlane, D. R., Elias, P., Geier, J. D., and Bolan, J. F. "ANL-6034 Design Summary Report On the Transient Reactor Test Facility (TREAT)", Argonne National Laboratory, Reactor-General (TID-4500, 15th Ed.), AEC R&D Report, June 1960, 85-86.
[9] Parga, C. J., van Rooyen, I. J., Glazoff, M. V., Luther, E. P. "TREAT reactor LEU fuel-clad chemical interaction empirical-modeling analysis" Conference Proceedings, ANS, Top Fuel, 2016, 1-20.
[10] Thermo-Calc v.2017b, Stockholm, Sweden, 2017.
[11] Guéneau C., Dupin, N., Martial, C., Dumas, J-C., Gossé, S., Chatain, S., Sundman, B. "Thermodynamic modelling of the U-Pu-O-C system using the Calphad method –Intermediate Report" CEA, F-BRIDGE-Document D-134–R0, Co-funded by the European Commission under the Euratom Research and Training Programme on Nuclear Energy within the Seventh Framework Programme, Contract No. 211690, 2010.
[12] Glazoff, M. V., van Rooyen, I. J., Coryell, B. D., Parga, C. J. "Comparison of Nuclear Fuels for TREAT: UO_2 vs U_3O_8" INL/EXT-16-37972, May 2016, 1-33.
[13] Parga, C. J. "TREAT LEU Fuel Assembly Cladding Oxidation" PLN-5398 r1, INL-MIS-16-40714, Dec. 2017, 1-53.
[14] Vandegrift, J. and Jaques, B. "Report on the Oxidation and Transient Testing of Zirconium Alloys" INL/INT-18-45726 r0, May 2018, 1-55.
[15] Okamoto, H., *J. Phase Equilib*., Vol 17 (No. 2), 1996, 162.
[16] C (Carbon) Binary Alloy Phase Diagrams, Alloy Phase Diagrams. Vol 3, ASM Handbook, ASM International, 2016, 218–228.
[17] Madelung O., ed., "Phase Equilibria, Crystallographic and Thermodynamic Data of Binary Alloys · B-Ba – C-Zr" Landolt-Börnstein - Group IV Physical Chemistry, Volume 5B, 1992.
[18] Sarian, S. and Criscione, J. M. "Diffusion of Carbon through Zirconium Monocarbide" J. of Applied Physics, vol. 38 no. 4, 1967, 1794-1798.